Bi@hemistry

pubs.acs.org/biochemistry Article

MA'AT Analysis of Aldofuranosyl Rings: Unbiased Modeling of Conformational Equilibria and Dynamics in Solution

Reagan J. Meredith, Margaret McGurn, Christopher Euell, Peter Rutkowski, Evan Cook, Ian Carmichael, and Anthony S. Serianni*



Cite This: Biochemistry 2022, 61, 239-251



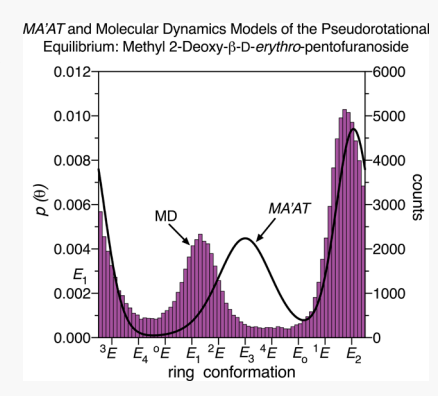
ACCESS I

III Metrics & More

Article Recommendations

s Supporting Information

ABSTRACT: *MA'AT* analysis has been applied to methyl β-D-ribofuranoside (3) and methyl 2-deoxy-β-D-erythro-pentofuranoside (4) to demonstrate the ability of this new experimental method to determine multi-state conformational equilibria in solution. Density functional theory (DFT) was used to obtain parameterized equations for >20 NMR spin-coupling constants sensitive to furanose ring conformation in 3 and 4, and these equations were used in conjunction with experimental spin-couplings to produce unbiased MA'AT models of ring pseudorotation. These models describe two-state north—south conformational exchange consistent with results obtained from traditional treatments of more limited sets of NMR spin-couplings (e.g., PSEUROT). While PSEUROT, MA'AT, and aqueous molecular dynamics models yielded similar two-state models, MA'AT analysis gives more reliable results since significantly more experimental observables are employed compared to PSEUROT, and no assumptions are needed to render the fitting tractable. MA'AT models indicate a roughly equal distribution of north



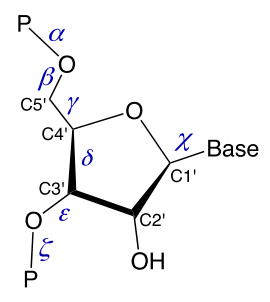
and south ring conformers of 4 in aqueous ($^2\text{H}_2\text{O}$) solution compared to \sim 80% north forms for 3. Librational motion about the mean pseudorotation phase angles P of the preferred north and south conformers of 3 in solution is more constrained than that for 4. The greater rigidity of the β -ribo ring may be caused by synergistic stereoelectronic effects and/or noncovalent (e.g., hydrogenbonding) interactions in solution that preferentially stabilize north forms of 3. MA'AT analysis of oligonucleotides and other furanose ring-containing biomolecules promises to improve current experimental models of sugar ring behavior in solution and help reveal context effects on ring conformation in more complex biologically important systems.

■ INTRODUCTION

Nucleic acids display various degrees of flexibility that are closely linked to their biological functions. For example, the binding of transcription factors and other proteins to DNA causes substantial bending of the phosphodiester backbone to allow binding and assembly of the multi-protein/enzyme transcriptional machinery. The rotational degrees of freedom of the phosphodiester backbone are dictated by six torsion angles (Scheme 1). Torsion angles γ and δ are directly associated with, and torsion angles β and ε are indirectly influenced by, furanose ring conformation. Significant backbone flexibility is conferred by furanose rings, which serve as transducers that connect backbone conformation and nitrogen base disposition. The latter disposition (quasi-axial/quasi-equatorial N-glycoside bond orientation) and syn/anti N-glycoside bond conformation (χ) are affected by furanose ring conformation.

To characterize DNA and RNA conformation and flexibility, a quantitative understanding of furanose ring conformational equilibria and dynamics is required. Furanose ring conformer exchange is energetically allowed due to the relatively low energy barriers (<3-4 kcal/mol) to nonplanar ring conformer exchange in solution. ^{6-83}E (C3'-endo) (north, N) \rightleftharpoons 2E (C2'-endo) (south, S) two-state conformational exchange (Scheme 2)

Scheme 1. Definitions of the Six Backbone Torsion Angles $(\alpha, \beta, \gamma, \delta, \varepsilon, \text{ and } \xi)$ in a Poly(ribo)nucleotide^a



^aTorsion angle χ describes the orientation of the nitrogen base relative to the sugar (N-glycoside conformation).

Received: September 22, 2021 Revised: January 11, 2022 Published: February 1, 2022





Scheme 2. Pseudorotational Itinerary of a D-Aldofuranose Ring^a

west
$$E_0$$
 1.5 P/π (radians) 0.5 P/π (radians) 0.7 E_1 E_2 0.7 E_1 E_3 0.7 E_4 E_4 0.7 E_1 E_4 0.8 E_4 0.7 E_1 E_4 0.9 E_4 0.9 E_4 0.7 E_1 E_4 0.9 E_4

"This circular pathway describes a mechanism of exchange between nonplanar conformers of the ring that does not require the involvement of the planar form.

is believed to accurately describe furanose behavior in singleand double-stranded DNA and RNA in solution based on statistical analyses of NMR and crystal structures. 4 Which of these two states is preferred depends on the type of DNA or RNA duplex (A- or B-type) and on other structural factors (e.g., single- vs double-stranded; hybrid duplexes). These conformational options are exploited, for example, in protein-nucleic acid recognition and in the mechanism of intramolecular catalysis by ribozymes. 10,11 In the latter case, furanose ring conformational change in the C residue at the cleavage site is critical to proper alignment of its O2' with an oxygen atom attached to phosphate on the adjacent C3', the latter eventually becoming O5' on the new 5'-end after cleavage (the two oxygens assume axial positions in the trigonal bipyramidal transition state of P). In this case, conversion of ³E (N form, C3'-endo, favored in groundstate A-RNA) (Scheme 2) to ²E (S form, C2'-endo) in the transition state is required for catalysis. 10 Presumably, the motional properties of the RNA backbone permit transient access to the ²E form, which then allows productive attack of the O2' nucleophile on phosphate to generate a penta-coordinate phosphate transition state and subsequent formation of a 2',3'cyclic phosphate intermediate. 11 Although not often considered in the mechanism, the conformation of the β -D-ribofuranosyl ring may also affect the p K_a of O2'H on the C residue, with a quasi-equatorial orientation of the C2'-O2' bond in ²E associated with a lower pK_a than the quasi-axial orientation of the same bond in ${}^{3}E$, possibly due to a shorter C-O bond in the former. This reduction in pK_a would promote hydroxyl hydrogen abstraction, thereby activating O2 as a nucleophile and promoting catalysis.

Conventional experimental conformational analyses of the β -D-ribofuranosyl (1) and 2-deoxy-eta-D-erythro-pentofuranosyl (2deoxy- β -D-ribofuranosyl) (2) rings of RNA and DNA, respectively, are based on the use of three-bond (vicinal) ${}^{1}H^{-1}H$ spin-coupling constants $({}^{3}J_{HH})$, intra-ring ${}^{1}H^{-1}H$ nuclear Overhauser effects (NOEs), ^{13–15} and in some cases CSA-dipolar cross-correlated relaxation. ^{16,17}PSEUROT¹⁸ uses ³J_{HH} values and a generalized Karplus equation¹³ to calculate the relative populations of north (N) (3E) and south (S) (2E) conformers in solution consistent with observations from statistical analyses of X-ray crystal structures and molecular dynamics (MD) simulations. The number of useful ${}^{3}J_{HH}$ values in 1 and 2 is limited to 3-5, and the cisoidal ${}^{3}J_{\rm H2,H3}$ in 1, and cisoidal ${}^{3}J_{H1,H2R}$ and ${}^{3}J_{H2S,H3}$ values in 2, are compromised by their more complex dependencies (bimodal) on ring conformation, limited dynamic ranges, and by the Barfield effect. 19,20 While the endocyclic torsion angles $\theta_0 - \theta_4$ (see 3 and 4) are interdependent, the number of useful ${}^{3}J_{HH}$ values is too small to determine solution conformation, especially for 1, unless a two-state $N \rightleftarrows S$ model is assumed (i.e., the problem is underdetermined). Conformational models involving three or more states in equilibrium cannot be treated easily. 21 To address the problem of underdetermination, ${}^{3}J_{HH}$ values are measured at different temperatures, but it is assumed that temperature affects only the relative populations of N and S forms and not mean pseudorotation phase angles P or puckering amplitudes $\tau_{\rm m}$. Initial pseudorotation parameters are set by the user at the start of PSEUROT analysis, and the user defines a subset of pseudorotation parameters that will be optimized to make the computations tractable. PSEUROT does not produce probability distribution models of ring conformation, that is, experimental plots of conformer probability vs P that are superimposable on similar plots obtained by computations such as MD simulation. While J_{CH} values have been measured in the furanose rings of oligonucleotides, 22-24 quantitative interpretations have not been reported. Systematic, quantitative studies of $J_{\rm CC}$ values in oligonucleotides are also lacking, despite their potential as furanose ring conformational constraints.

OH
H5S
H5R
$$\theta_2$$
 θ_3
 θ_4
H1
H0
OH
methyl θ_1 -D-ribofuranoside (3)
OH
H5S
H3
H2
 θ_4
H1
H0
H2R
methyl 2-deoxy- θ_1 -D-erythropentofuranoside (4)

The present work describes the application of a new experimental method, MA'AT analysis, $^{26-30}$ to investigate furanose ring conformation and dynamics in solution (the method is named after the Egyptian goddess, MA'AT). An advantage of this method is that the assumption of a two-state $^{3}E/^{2}E$ model, or indeed of any potential model, is not required to fit the experimental data, and computational data (e.g., MD simulations) are not required to assist in the interpretation of experimental data. MA'AT analysis was applied to two model furanoses, methyl β -D-ribofuranoside (3) and methyl 2-deoxy- β -

D-erythro-pentofuranoside (4), with the expectation that successful modeling of these simple rings will be extendable to more complex systems containing spin-isolated furanosyl ring constituents (e.g., DNA and RNA oligonucleotides; furanose-containing oligosacharides). We show here, for the first time, that MA'AT analysis can treat multi-state conformational equilibria, thereby broadening its applicability beyond the single-state treatments described previously^{26–30} to conformational elements in saccharides and other biomolecules such as exocyclic hydroxymethyl group conformation, exocyclic C–O bond conformation, and pyranosyl ring pseudorotation, where two or more conformational states are likely to coexist in chemical exchange in solution.

EXPERIMENTAL SECTION

Experimental NMR Spin-Coupling Constants in 3 and 4. All NMR spin-coupling constants (J_{HH} , J_{CH} , and J_{CC}) used in MA'AT analyses of 3 and 4 were taken from prior work.²⁵

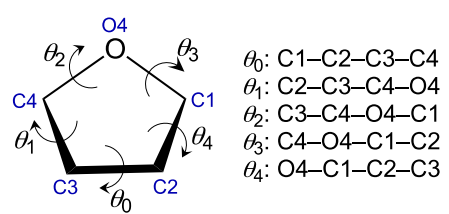
COMPUTATIONAL METHODS

Geometry Optimizations. Density functional theory (DFT) calculations were conducted within $Gaussian16^{31}$ using the B3LYP functional^{32,33} and the 6-31G* basis set³⁴ for geometric optimization. Twenty-one initial structures of 3^c and 4^c (the superscript "c" denotes an in silico structure, to be distinguished from the chemical compounds 3 and 4) were built using GaussView corresponding to the 10 envelopes (E), 10 twists (T), and planar conformers as defined by the Altona-Sundaralingam^{35,36} pseudorotation model for five membered rings. Each ring conformer, except for the planar form, has a unique pseudorotational phase angle, P, that specifies the ring atoms that are displaced out of the plane defined by three (T forms) or four (E forms) contiguous atoms in the ring. The puckering amplitude, τ_m , defines the extent to which the atoms are displaced from this plane. Equation 1 was used to calculate P from the five endocyclic torsion

$$\tan P = \frac{(\theta_2 + \theta_4) - (\theta_1 + \theta_3)}{3.077\theta_0} \tag{1}$$

angles defined in Scheme 3 and eq 2 was used to calculate $\tau_{\rm m}$. Initial and optimized puckering parameters, P and $\tau_{\rm m}$, for 3° and

Scheme 3. Definitions of the Endocyclic Torsion Angles θ_0 – θ_4 Used in Eqs 1 and 2



4° are listed in Table S1 (see the Supporting Information). Exocyclic torsional constraints in 3° and 4° that were applied during geometry optimization are summarized

$$\tau_{\rm m} = \frac{\theta_0}{\cos P} \tag{2}$$

in Schemes S1 and S2 and Table S2 (see the Supporting Information). During geometric optimization, two of the five endocyclic torsion angles were fixed to ensure that the *in silico*

structure retained its initial ring conformation. For 3^c and 4^c, the exocyclic C1–C2–O2–H (3^c only), C2–C3–O3–H, and C3–C4–C5–O5 torsion angles were rotated in 60° increments through 360° to produce ring conformers containing different combinations of staggered and eclipsed C–O and C–C rotamers. All remaining geometric parameters were optimized. These calculations produced 4536 optimized structures of 3^c and 756 optimized structures of 4^c. Geometry calculations included the effects of solvent water, which were treated using the self-consistent reaction field (SCRF)³⁷ and the integral equation formalism (polarizable continuum) model (IEFPCM)³⁸ as implemented in *Gaussian*16.

Calculations of NMR Spin-Coupling Constants. $J_{\rm HH}$, $J_{\rm CH}$, and $J_{\rm CC}$ values were calculated in geometry-optimized structures of 3° and 4° using $Gaussian16^{31}$ and DFT. 32,33 The Fermi contact, $^{39-41}$ diamagnetic and paramagnetic spin-orbit, and spin-dipole 39 terms for each J-coupling were calculated using the B3LYP functional and a tailored [5s2p1dl3s1p] basis set, 42,43 and raw (unscaled) calculated J-couplings are reported. All spin-coupling constant calculations included the effects of solvent water, which were treated using the self-consistent reaction field (SCRF) 37 and the integral equation formalism (polarizable continuum) model (IEFPCM) 38 as implemented in Gaussian16.

Prior work in this laboratory using the B3LYP functional and $6\text{-}31G^*$ basis set to obtain optimized geometries, and the B3LYP functional and [5s2p1dl3s1p] basis set to calculate J_{HH} , J_{CH} , and J_{CC} values, has shown that J-couplings calculated in this manner have errors of <5% when secondary effects on their magnitudes are accounted for, and when only geminal (2J) or vicinal (3J) values are considered. The latter longer-range J-couplings are relatively small in magnitude, ranging in absolute value from 0 to 10 Hz on average, translating into absolute errors of $\pm 0.2 - 0.3$ Hz in most cases. These errors are comparable to those associated with the experimental J-couplings and have been found not to significantly affect the results of MA'AT modeling.

NMR Spin-Coupling Equation Parameterization. Equations relating DFT-calculated spin-couplings in 3^{c} and 4^{c} to pseudorotational phase angle, P, were parameterized using all geometry-optimized structures except those having relative energies greater than 10 kcal/mol, as described previously. The latter cutoff was applied to remove structurally distorted conformers whose inclusion would adversely affect equation parameterization. Plots of J-couplings in structures 3^{c} and 4^{c} as a function of P (Scheme 3) were parameterized and are found in the Supporting Information (eqs S1–S58). The curves were fit to the following modified Karplus-like equation (eq 3) using R.

$${}^{n}J_{X,Y} (Hz) = k + a \cos \theta + b \sin \theta + c \cos 2\theta + d \sin 2\theta$$
(3)

This generalized form of the Karplus-like equation was first described by Pachler. ⁴⁴ He proposed the use of this trigonometric function to account for asymmetry in the Karplus curve caused by the substitution of a hydrogen atom in the coupling pathway. This trigonometric polynomial form was adopted because it provides the best parameterization to the DFT data with the smallest number of terms. This form of the equation is also amenable to simple integration, making it compatible with MA'AT analysis ^{26–30} for modeling torsional populations in solution. The goodness-of-fit of each equation was expressed as a root-mean-square deviation (RMSD).

Aqueous Molecular Dynamics Simulations of 3^c and 4^c. Initial structures of 3^c and 4^c were built using the Carbohydrate Builder module available at the GLYCAM website (http://www.glycam.org).⁴⁵ The GLYCAM06⁴⁶ (version j) force field was employed in all simulations. Structures 3° and 4° were solvated with TIP3P⁴⁷ water using a 12 Å buffer in a cubic box and the LEaP module in the AMBER14 software package. 48 Energy minimizations for solvated 3° and 4° were performed separately under constant volume (500 steps steepest descent, followed by 24 500 steps of conjugate-gradient minimization). Each system was subsequently heated to 300 K over a period of 50 ps, followed by equilibration at 300 K for a further 0.5 ns using the nPT condition, with the Berendsen thermostat⁴⁹ for temperature control. All covalent bonds involving hydrogen atoms were constrained using the SHAKE algorithm, ⁵⁰ allowing a simulation time step of 2 fs throughout the simulation. After equilibration, production simulations were carried out with the graphics processing unit (GPU) implementation⁵¹ of the PMEMD.MPI module and trajectory frames were collected every 1 ps for a total of 1 μ s. One to four nonbonded interactions were not scaled,⁵² and a nonbonded cutoff of 8 Å was applied to van der Waals interactions, with long-range electrostatics treated with the particle mesh Ewald approximation. Output from each MD simulation was imported into Prism⁵³ for visualization.

RESULTS AND DISCUSSION

Spin-Coupling Ensembles in Methyl β -D-Ribofuranoside (3) and Methyl 2-Deoxy- β -D-erythro-pentofuranoside (4)—General Considerations. Furanosides 3 and 4 contain 28 and 35 spin-coupling constants, respectively, that are potentially sensitive to ring endocyclic torsion angles θ_0 – θ_4 (Scheme 3 and Tables 1 and 2). Conventional determinations of

Table 1. NMR Spin-Coupling Constants Sensitive to Ring Endocyclic Torsion Angles $\theta_0-\theta_4$ in Methyl β -D-Ribofuranoside (3)

Spin-Coupling Constants in 3								
$^{3}J_{\rm HH}$	$^{1}J_{CH}$	$^2J_{\rm CH}$	$^{3}J_{\mathrm{CH}}$	¹Jcc	$^{3}J_{CC}$	$^{2+3}J_{\rm CC}^{d}$		
$J_{\text{H1,H2}\atop (\boldsymbol{\theta_4})^a}$	$^{1}J_{C1,H1}$	$^2J_{C1,H2}$	$J_{\text{C1,H3}} \begin{pmatrix} \theta_0 \end{pmatrix}$	$^{1}J_{C1,C2}$	$J_{\text{C1,C5}} (\boldsymbol{\theta_2})$	$^{2+3}J_{C1,C3}$		
$(\boldsymbol{\theta_0})^{3}$	$^{1}J_{C2,H2}$	$^{2}J_{C2,H1}$	$J_{\text{C1,H4}} \atop (\boldsymbol{\theta_2})$	$^{1}J_{C2,C3}$	$J_{\text{C2,C5}} \atop (\boldsymbol{\theta_1})$	²⁺³ J _{C1,C4}		
$\overset{^{3}J_{\mathrm{H3,H4}}}{(\boldsymbol{\theta_{1}})}$	$^{1}J_{C3,H3}$	$^{2}J_{\text{C2,H3}}$	$J_{\text{C2,H4}} \atop (\boldsymbol{\theta_1})$	$^{1}J_{C3,C4}$		$^{2+3}J_{C2,C4}$		
	¹J _{C4,H4}	$^{2}J_{C3,H2}$	$J_{\text{C3,H1}} (\boldsymbol{\theta_4})$					
		$^{2}J_{C3,H4}$	$J_{\text{C4,H1}} (\boldsymbol{\theta}_3)$					
		$^{2}J_{C4,H3}$	$J_{\text{C4,H2}} (\boldsymbol{\theta_0})$					
			$^{3}J_{\text{CS,H3}} $ $(\boldsymbol{\theta}_{1})$					
Subtotals of Spin-Coupling Constants in 3								
3	4	6	7	3	2	3		
Total Spin-Couplings = 28 ^b								
³ J Values Only: ^c 12 Spin Couplings $(3\theta_0, 4\theta_1, 2\theta_2, 1\theta_3, 2\theta_4)$								

"In parentheses: the endocyclic torsion angle in 3 that can be evaluated by the indicated *J*-coupling. "The sum of all *J*-couplings in 3 that can be used, in principle, to evaluate ring conformation. "The total number of vicinal *J*-couplings in 3 that are expected to depend strongly on specific endocyclic torsion angles. "Dual-pathway *J*-couplings.

ring conformation in 3 in solution use three ${}^3J_{\rm HH}$ values (\sim 11% of 28), whereas five ${}^3J_{\rm HH}$ values (\sim 14% of 35) are used for similar determinations in 4. Significant structural information encoded in numerous *J*-couplings in these rings has largely remained untapped.

The 28 *J*-couplings in 3 fall into seven groups: ${}^3J_{\text{HH}}$, ${}^1J_{\text{CH}}$, ${}^2J_{\text{CH}}$, ${}^3J_{\text{CH}}$, ${}^1J_{\text{CC}}$, and ${}^{2+3}J_{\text{CC}}$ (Table 1). The vicinal *J*-couplings (total of 12) can be further distinguished based on differences in their coupling pathways: ${}^3J_{\text{HCCH}}$, ${}^3J_{\text{CCCH}}$, ${}^3J_{\text{COCH}}$, ${}^3J_{\text{CCCC}}$, and ${}^3J_{\text{COCC}}$. The vicinal *J*-couplings have positive signs, and their magnitudes depend heavily on the torsion angle subtended by the coupled nuclei (Karplus dependencies ${}^{54-57}$). Specific 3J values can therefore be associated with specific ring endocyclic torsion angles $\theta_0 - \theta_4$ (Table 1) with a high degree of confidence. This study aimed to apply these 3J values collectively to model ring conformation in 3.

While not investigated herein, some of the 16 remaining Jcouplings may be useful as additional conformational constraints in 3 or in the β -D-ribofuranosyl rings (see structure 1) of ribonucleosides/tides and oligoribonucleotides. ¹J_{CH} values in aldofuranosyl rings depend on C-H bond orientation. ⁵⁸ A given C-H bond can adopt either a quasi-axial or quasi-equatorial orientation depending on furanosyl ring conformation. For example, the C1-H1 bond is quasi-axial in E_1 and quasiequatorial in ¹E (Scheme 2). All else being equal, a given C-H bond is typically longer when quasi-axial than when quasiequatorial, and the associated ${}^{1}J_{CH}$ (ax) will be smaller than ${}^{1}J_{CH}$ (eq) (Scheme 4) (longer C–H bonds have less s-character and yield smaller ${}^{1}J_{CH}$ values). ⁵⁹ However, as generally observed for ¹J and ²J values in saccharides and complicating their interpretation in conformational terms, additional structural factors affect ¹J_{CH} magnitudes, such as vicinal lone-pair effects involving either the ring oxygen (which reinforce the abovenoted bond orientation effects) or the oxygens of exocyclic hydroxyl groups (Scheme 4).⁶⁰ Similar behaviors are observed for ${}^{1}J_{CC}$ in vicinal diol fragments. 61 For example, ${}^{1}J_{C1,C2}$ in 3 is influenced not only by θ_4 (i.e., rotation about the C1–C2 bond) but also by rotations about the C1-O1 and C2-O2 bonds, with the effects of the latter rotations stronger than rotation about θ_4 (Scheme 5).61

 $^2J_{\rm CCH}$ values are also likely to show useful dependencies on $\theta_0-\theta_4$ since they are affected by the relative orientations of electronegative atoms appended to the C–C fragment. These relative orientations change as 3 undergoes pseudorotation. For a fixed combination of exocyclic C–O bond torsions, $^2J_{\rm CCH}$ values in 3 show a nearly linear dependence on specific endocyclic torsion angles (Figure S5, Supporting Information). However, like $^1J_{\rm CH}$ and $^1J_{\rm CC}$, exocyclic C–O bond rotation influences $^2J_{\rm CCH}$ values, especially C–O bond rotations involving the carbon bearing the coupled hydrogen. 62

In 3, three dual-pathway $^{13}C^{-13}C$ spin couplings $(^{2+3}J_{CC})$ exist between C1 and C3, C1 and C4, and C2 and C4, each involving two pathways, one geminal (for $^{2+3}J_{C1,C3}$, C1–C2–C3) and the other vicinal (for $^{2+3}J_{C1,C3}$, C1–O4–C4–C3). The structural dependencies of dual-pathway $^{13}C^{-13}C$ spin couplings in saccharides have been investigated using conformationally defined model compounds 63 and are generally small, making them less attractive for MA'AT modeling of aldofuranosyl rings.

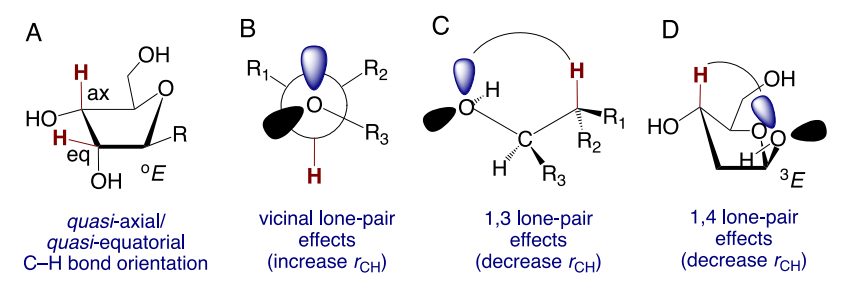
The structural dependencies of spin-couplings in 3 discussed above also apply to 4 (Table 2). In the present work, $15^{3}J$ values are available for MA'AT modeling of 4 given their strong and

Table 2. NMR Spin-Coupling Constants Sensitive to Ring Endocyclic Torsion Angles $\theta_0 - \theta_4$ in Methyl 2-Deoxy- β -D-erythropentofuranoside (4)

Spin-Coupling Constants in 4									
$^2J_{\rm HH}$	³ Ј _{нн}	¹J _{CH}	$^2J_{\mathrm{CH}}$	³ J _{CH}	¹Jcc	³Jcc	$^{2+3}J_{\rm CC}^{d}$		
² J _{H2R,H2S}	$^{3}J_{\text{H1,H2R}}(\theta_{4})^{a}$ $^{3}J_{\text{H1,H2S}}(\theta_{4})$ $^{3}J_{\text{H2R,H3}}(\theta_{0})$ $^{3}J_{\text{H2S,H3}}(\theta_{0})$ $^{3}J_{\text{H3,H4}}(\theta_{1})$	¹ J _{C1,H1} ¹ J _{C2,H2R} ¹ J _{C2,H2S} ¹ J _{C3,H3} ¹ J _{C4,H4}	² J _{C1,H2R} ² J _{C1,H2S} ² J _{C2,H1} ² J _{C2,H3} ² J _{C3,H2R} ² J _{C3,H2S} ² J _{C3,H4} ² J _{C4,H3} ubtotals of Spin-Co	$^{3}J_{\text{C1,H3}}(\theta_{0})$ $^{3}J_{\text{C1,H4}}(\theta_{2})$ $^{3}J_{\text{C2,H4}}(\theta_{1})$ $^{3}J_{\text{C3,H1}}(\theta_{4})$ $^{3}J_{\text{C4,H1}}(\theta_{3})$ $^{3}J_{\text{C4,H2R}}(\theta_{0})$ $^{3}J_{\text{C4,H2S}}(\theta_{0})$ $^{3}J_{\text{C5,H3}}(\theta_{1})$ upling Constants in 4	¹ Jc1,c2 ¹ Jc2,c3 ¹ Jc3,c4	$^{3}J_{\text{C1,CS}}\left(\boldsymbol{\theta}_{2}\right)$ $^{3}J_{\text{C2,CS}}\left(\boldsymbol{\theta}_{1}\right)$	2+3 <i>J</i> C1,C3 2+3 <i>J</i> C1,C4 2+3 <i>J</i> C2,C4		
1	5	5	8 Total Spin Co	8 souplings = 35^b	3	2	3		
3J Values Only: c 15 Spin Couplings (5 $ heta_0$; 4 $ heta_1$; 2 $ heta_2$; 1 $ heta_3$; 3 $ heta_4$)									

"In parentheses: The endocyclic torsion angle in 4 that can be evaluated by the indicated *J*-coupling. "The sum or all *J*-couplings in 4 that can be used, in principle, to evaluate ring conformation. "The total number of vicinal *J*-couplings in 4 that are expected to depend strongly on specific endocyclic torsion angles. "Dual-pathway *J*-couplings."

Scheme 4. Bond Orientation (A) and Oxygen Lone-Pair Effects (B–D) that Influence C–H Bond Lengths and ${}^{1}J_{CH}$ Values in Saccharides^a



"Pseudorotation of the ring in (A) allows a given C-H bond to adopt quasi-axial or quasi-equatorial orientations, which affects their lengths and corresponding ${}^{1}J_{CH}$ values. The effects shown in (A)-(D) collectively determine C-H bond lengths and thus ${}^{1}J_{CH}$ magnitudes in furanosyl rings.

Scheme 5. ¹J_{CC} Behavior in Vicinal Diol Fragments^a

 $^{a1}J_{C_aC_b}$ depends on rotation about α but is also strongly influenced by rotations about β and γ . The effects of the latter rotations are caused by oxygen lone-pair orbital interactions with covalent bonds in the HO–C_a–C_b–OH fragment (vicinal effects on the C_a–C_b bond length).

essentially singular dependencies on specific endocyclic torsion angles $\theta_0-\theta_4$, but additional *J*-values may prove useful in *MA'AT* modeling of the 2-deoxy- β -D-erythro-pentofuranosyl ring in 2′-deoxyribonucleosides/tides, 2′-deoxyribooligonucleotides, and related systems. In oligoribonucleotides and oligodeoxyribonucleotides, conformations about the C3′-O3′ bonds of each residue are often highly constrained by oligomer backbone conformation, thus potentially simplifying conformational interpretations of ${}^1J_{\rm CH}$, ${}^1J_{\rm CC}$, and ${}^2J_{\rm CCH}$ values in these rings by eliminating lone-pair effects arising from O3′.

Parameterization of Equations for Geminal and Vicinal ¹H-¹H, ¹³C-¹H, and ¹³C-¹³C Spin-Coupling Constants in 3 and 4. A wide range of *J*-couplings potentially sensitive to ring conformation in 3 and 4 was investigated by DFT to determine the degree to which they depend on

pseudorotational phase angle, *P*. These dependencies are shown in Figures S1—S4 in the Supporting Information. Parameterized equations for each *J*-value were obtained from the fitting of these plots (see eqs S1—S58 in the Supporting Information). Based on these results, 20 and 22 redundant *J*-couplings were found to be sufficiently sensitive to pseudorotation phase angle *P* in 3 and 4, respectively, and relatively unaffected by secondary structural effects to render them useful in *MA'AT* analyses. For 3, these *J*-values included ${}^{3}J_{\text{H1,H2}}$ ${}^{3}J_{\text{H2,H3}}$, ${}^{3}J_{\text{H2,H3}}$, ${}^{3}J_{\text{C3,H1}}$, ${}^{2}J_{\text{C2,H1}}$, ${}^{2}J_{\text{C2,H3}}$, ${}^{3}J_{\text{C3,H2}}$, ${}^{2}J_{\text{C3,H2}}$, ${}^{3}J_{\text{C1,H3}}$, ${}^{3}J_{\text{C1,H3}}$, ${}^{3}J_{\text{C1,H4}}$, ${}^{3}J_{\text{C3,H1}}$, ${}^{3}J_{\text{C4,H1}}$, ${}^{3}J_{\text{C4,H2}}$, ${}^{3}J_{\text{C1,H2}}$, ${}^{3}J_{\text{C1,H2}}$, ${}^{3}J_{\text{C1,H3}}$, ${}^{3}J_{\text{C1,H3}}$, ${}^{3}J_{\text{C1,H3}}$, ${}^{3}J_{\text{C1,H3}}$, ${}^{3}J_{\text{C1,H3}}$, ${}^{3}J_{\text{C1,H3}}$, ${}^{3}J_{\text{C1,H4}}$, ${}^{3}J_{\text{C1,H4}}$, ${}^{3}J_{\text{C1,H4}}$, ${}^{3}J_{\text{C1,H1}}$, ${}^{3}J_{\text{C1,H2}}$, ${}^{3}J_{\text{C1,H2}}$, ${}^{3}J_{\text{C1,H2}}$, ${}^{3}J_{\text{C1,H2}}$, ${}^{3}J_{\text{C1,H2}}$, ${}^{3}J_{\text{C1,H3}}$, ${}^{3}J_{\text{C2,C5}}$, and ${}^{2+3}J_{\text{C1,C4}}$ (Table S4, Supporting Information).

MA'AT Modeling of Ring Conformation and Dynamics in 3 and 4 and Comparison to Models Obtained by Aqueous MD Simulations. Different ensembles of experimental *J*-values (Table 3) were used to model ring conformation in 3 and 4 using MA'AT analysis to determine the degree to which the models are affected by the ensemble used in the analysis. The results of this modeling are shown in Figures 1–4. For 3, nine different ensembles of *J*-values (see Table S3, Supporting Information, to identify which *J*-values were used in each fit) yielded nine similar two-state models describing an exchange between ring conformations with mean

Table 3. $^{1}\text{H}-^{1}\text{H}$, $^{13}\text{C}-^{1}\text{H}$, and $^{13}\text{C}-^{13}\text{C}$ Spin Couplings a in Methyl β -D-Ribofuranoside (3) and Methyl 2-Deoxy- β -D-erythro-pentofuranoside (4)

	compound			
<i>J</i> -coupling	3	4		
$^{2}J_{H2R,H2S}$		-13.9		
$^{3}J_{\rm H1,H2}$	1.2			
$^{3}J_{\rm H1,H2R}$		5.4		
$^{3}J_{\mathrm{H1,H2S}}$		2.6		
$^{3}J_{\rm H2,H3}$	4.6			
$^{3}J_{H2R,H3}$		5.7		
$^{3}J_{\text{H2S,H3}}$		6.7		
$^{3}J_{\rm H3,H4}$	6.9	4.2		
$^{1}J_{\mathrm{C1,H1}}$		173.9		
$^{2}J_{\mathrm{C1,H2}}$	0			
$^{2}J_{C1,H2R}$		-1.5		
² J _{C1,H2S}		-4.6		
²J _{С2,Н1}	-0.8			
$^{2}J_{C2,H3}$	1.2			
$^{2}J_{C3,H2}$	0.7			
$^{2}J_{C3,H2R}$		-6.4		
$^{2}J_{C4,H3}$	-0.7	1.5		
³J _{C1,H3}	1.2	2.7		
$^{3}J_{C1,H4}$	2.9	4.8		
$^{3}J_{C2,H4}$	0.9	1.2		
³J _{C3,H1}	3.1	3.3		
$^{3}J_{C4,H1}$	4.5	5.0		
$^{3}J_{C4,H2}$	4.3			
$^{3}J_{C4,H2R}$		2.0		
$^{3}J_{C4,H2S}$		4.2		
³ J _{С5,Н3}	4.8	4.0		
$^{2}J_{C3,C5}$	2.3			
$^{3}J_{C1,C5}$	0.5	0		
³ J _{C2,C5}	1.8	1.1		
²⁺³ J _{C1,C3}	3.0			
²⁺³ J _{C1,C4}	0	0		

^aln Hz at ~25 °C in 2 H₂O solvent; ± 0.1 Hz; data taken from ref 25. Spin-coupling values of 0 Hz were used in *MA'AT* analyses when no discernible line splitting was observed in 1 H and 13 C NMR spectra, indicating that the experimental value is <0.7 Hz but not necessarily 0.

P values between 353-359° (N forms) and 171-189° (S forms), giving average P values of 355 and 179°, respectively, which correspond to the 3T_2 (N) and 2T_3 (S) conformers, respectively (Scheme 2, Figure 1, and Table 4). North conformers are significantly more abundant (77 \pm 1%) than south conformers (23 ± 1%). Circular standard deviations (CSDs) calculated for the N and S forms are comparable (11 \pm 5 and $10 \pm 4^{\circ}$, respectively). RMSD values calculated from each of the nine MA'AT models ranged from 0.3 to 0.6 Hz, giving an average RMSD of 0.45 ± 0.13 Hz. Good agreement was observed between the average MA'AT model of 3 and that determined by MD simulation, especially with respect to the mean P values of N and S forms (differences of $5-7^{\circ}$) (Table 4 and Figure 2). The equilibrium distribution of N and S forms determined by MD is also similar to that determined by MA'AT analysis (differences of <2% for each state). Significant differences, however, were observed between the MA'AT and MD models of 3 with respect to CSDs, with the former giving smaller values by 10-20°. MA'AT analysis indicates less

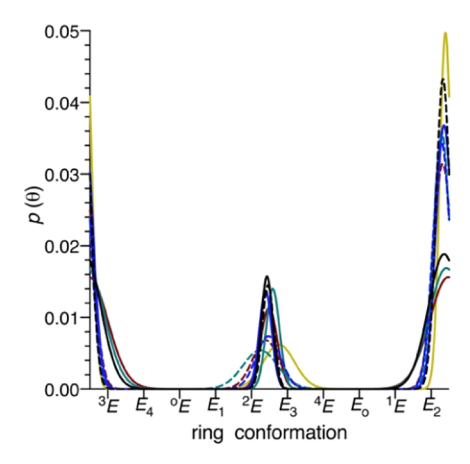


Figure 1. *MA'AT* modeling of methyl β-D-ribofuranoside (3) ring conformation in aqueous solution using nine different ensembles of redundant spin-coupling constants (see Tables 4 and S3). Fit 1, solid black; fit 2, dashed black; fit 3, solid blue; fit 4, dashed blue; fit 5, solid green; fit 6, dashed green; fit 7, solid red; fit 8, dashed red; and fit 9, solid yellow. Statistical parameters of each fit are given in Table 4.

conformational mobility about the mean P values for N and S forms than predicted by MD simulation. The RMSD calculated from the MD model (0.65 Hz) is larger on average than those obtained from the MA'AT models (0.45 \pm 0.13 Hz), indicating a better fit of the MA'AT models to the experimental J-couplings.

For 4, 13 different ensembles of *J*-couplings gave 13 very similar two-state models involving an exchange between ring conformations having mean P values between 336-357° and $192-207^{\circ}$, yielding average values of 345 ± 5 and $198 \pm 5^{\circ}$, respectively, that correspond to E_2 (north) and E_3 (south) conformers, respectively (Scheme 2, Figure 3, and Table 5). North conformers are slightly more abundant (58 \pm 3%) than south conformers (42 \pm 3%), and approximately 2-fold more S form is found in aqueous solution than found for 3. The average CSD value for N forms $(25 \pm 5^{\circ})$ is smaller than that for S forms $(41 \pm 3^{\circ})$. RMSD values calculated from the 13 models ranged from 0.1 to 0.5 Hz, giving an average of 0.34 \pm 0.14 Hz. Agreement between the MA'AT models of 4 and that obtained by MD simulation was fair with regard to the mean P values of N and S forms. For N forms, MD gave a mean value of 338°, in close agreement with MA'AT analysis (345 \pm 5°). However, MD simulation gave a mean value of 137° for S forms, while MA'AT analyses yielded an average value of 198 \pm 5°, a difference of ~61°. MD gave a slightly larger CSD for S forms (33°) than for N forms (27°) , in qualitative agreement with MA'AT results. However, the calculated RMSD for the MD model (0.74 Hz) was significantly larger than the average RMSD obtained from MA'AT analyses (0.34 \pm 0.14 Hz), indicating a poorer fit to the experimental J-couplings compared to the MA'AT models.

MA'AT Discrimination between Different Conformational Models of Furanose Rings. As shown above, *MA'AT* modeling of furanose ring conformation in 3 and 4 provides unbiased ring conformer probability distributions involving a two-site exchange between north and south ring conformers. Efforts to treat the *J*-coupling data for 3 and 4 using a one-state model gave poorer fits of the data than obtained when two-state modeling was allowed. When a three-state model was allowed, two-state N/S models identical to those shown in Figures 1–4 were obtained, indicating that three-state models could not be found that fit the data better than the two-state models.

Table 4. MA'AT Modeling Results for Methyl β -D-Ribofuranoside (3) Obtained Using Different Combinations of Redundant J-Couplings Sensitive to Ring Conformation

fit ^a	number of J-values	mean 1 (deg) ^e	CSD 1 (deg) ^e	mean 2 (deg) ^e	CSD 2 (deg) ^e	peak 1 (%) ^f	peak 2 (%) ^f	RMSD (Hz) ^g
1	19	355.1	16.2	177.5	5.7	77.5	22.5	0.64
2	16	354.0	7.0	178.5	5.8	78.9	21.1	0.64
3	15	354.9	8.2	176.0	6.2	78.6	21.4	0.57
4	13	352.5	8.7	178.8	12.4	77.2	22.8	0.33
5	12	357.3	17.9	183.3	6.7	76.5	23.5	0.41
6	12	352.6	8.2	170.8	17.8	76.1	23.9	0.34
7	12	359.2	19.4	179.5	8.3	76.4	23.6	0.43
8	11	353.6	9.5	176.4	13.5	77.1	22.9	0.34
9	7	356.4	5.7	189.4	16.0	75.3	24.7	0.32
avg^b		355.1	11.2	178.9	10.3	77.0	23.0	0.45
STD^c		2.1	4.9	4.9	4.4	1.1	1.1	0.13
MD^d		350.1	22.3	171.5	28.9	78.3	21.7	0.65

"Nine different combinations of *J*-couplings used to model ring conformation; the *J*-values used in each fit are given in Table S3 in the Supporting Information. "Averaged values obtained for the nine MA'AT fits. "STD = standard deviation." Obtained from a 1 μ s aqueous molecular dynamics simulation of 3 (see text for details). "Mean 1 and CSD 1 were calculated from peak 1; mean 2 and CSD 2 were calculated from peak 2. "Obtained from integration of peaks 1 and 2 obtained from MA'AT modeling or MD simulation. "RMSD = root-mean-square deviation."

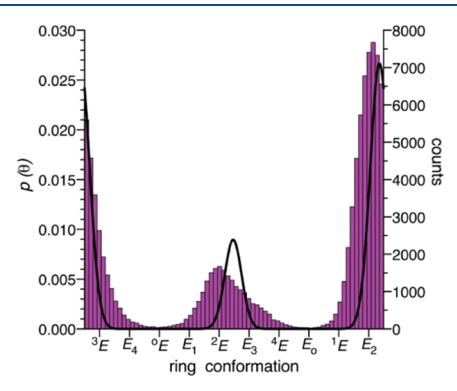


Figure 2. Overlay of the MA'AT model of furanose conformation in 3 with that obtained from aqueous molecular dynamics simulation (1 μ s; GLYCAM06). The black curve represents the MA'AT model obtained by averaging the nine models derived from the fits of nine different ensembles of J-couplings (see Figure 1 and Table 4). The hatched area in purple denotes the MD model.

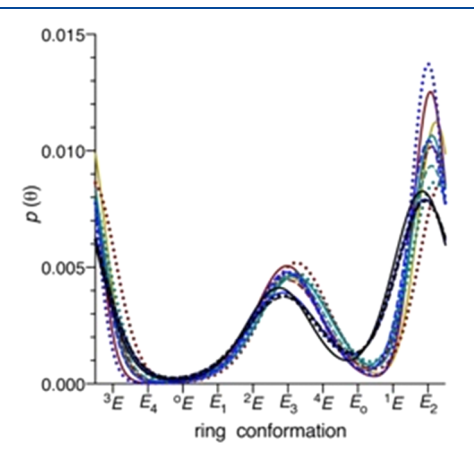


Figure 3. MA'AT modeling of methyl 2-deoxy-β-D-erythro-pentofuranoside (4) ring conformation in aqueous solution using 13 different ensembles of redundant spin-coupling constants (see Tables 5 and S4). Fit 1, solid black; fit 2, dashed black; fit 3, dotted black; fit 4, solid blue; fit 5, dashed blue; fit 6, dotted blue; fit 7, solid green; fit 8, dashed green; fit 9, dotted green; fit 10, solid red; fit 11, dashed red; fit 12, dotted red; and fit 13, solid yellow. Statistical parameters of each fit are given in Table 5.

The two-state MA'AT model for 3 describes ${}^3T_2 \leftrightarrows {}^2T_3$ exchange (Figure 2), whereas that for 4 describes $E_2 \leftrightarrows E_3$ exchange (Figure 4). Unlike other experimental approaches, the MA'AT method uses ensembles of redundant spin-couplings to generate single- ${}^{24-28}$ and multi-state probability distribution models of ring conformation with minimal bias and assumptions about the nature of the model. The furanosyl ring conformational equilibria determined for 3 and 4 describe typical N/S exchange in solution, consistent with conclusions drawn previously using simpler treatments of NMR J-couplings and other experimental parameters. 4,13,15,16

The applicability and reliability of MA'AT analysis to model furanosyl ring conformation in solution was tested by evaluating whether the method can distinguish between a two-state N/S model of ring conformational exchange and a single-state model comprised only of east conformers. While N/S exchange is believed to occur by pseudorotation via east (°E) conformers, the population of east forms in solution is believed to be low based on experimental⁶ and computational⁶⁴ studies, at least in simple furanose ring-containing compounds. However, in more complex structures such as DNA/RNA hybrid duplexes, N/S exchange in the DNA residues is absent and ${}^{\circ}E/E_1$ forms are preferred, whereas the RNA residues highly prefer ³E (north) conformations. 65 Experimental and computational (MD simulation⁶⁵) studies indicate that, at least in simple systems, °E forms are less stable than N and S forms by ~4.5 kcal/mol, and that N/S exchange via east forms may involve a significant reduction in puckering amplitude $(\tau_{\rm m})^{.64}$ If the latter pertains and were taken to the limit (i.e., $\tau_{\rm m} = 0^{\circ}$ in *E* forms), then N/S exchange via ring inversion (i.e., exchange through a planar intermediate) would compete with pseudorotation as a pathway for N/S exchange.

Two conformational exchange scenarios were examined to determine whether MA'AT modeling could shed light on the role of east conformations in RNA and DNA structure and function. A classical two-state N/S model involving 3E ($P=18^\circ$) and 2E ($P=162^\circ$) and a single-state 6E model ($P=90^\circ$) were examined (Scheme 2). In the $^3E \leftrightarrows ^2E$ model, equal populations of each conformer were assumed, and CSDs for both populations, and for the population in the single-state 6E model, were set at 30° . Ensembles of J-couplings in 3 and 4 were then back-calculated based on the assumed models and

Table 5. MA'AT Modeling Results for Methyl 2-Deoxy-β-D-erythro-pentofuranoside (4) Obtained Using Different Combinations of Redundant *J*-Couplings Sensitive to Ring Conformation

fit ^a	number of J-values	mean 1 (deg) ^e	CSD 1 $(deg)^e$	mean 2 (deg) ^e	CSD 2 (deg) ^e	peak 1 (%) ^f	peak 2 (%) ^f	RMSD (Hz) ^g
1	22	336.1	31.8	188.6	37.5	63.7	36.3	0.48
2	19	340.1	32.0	194.1	46.0	60.6	39.4	0.49
3	18	338.9	32.7	191.7	43.7	61.8	38.2	0.51
4	17	339.0	32.1	193.2	42.8	61.3	38.7	0.52
5	16	342.9	22.1	196.9	37.9	57.3	42.7	0.30
6	16	342.2	16.9	199.4	371.	58.2	41.8	0.22
7	15	346.1	20.7	205.1	41.9	54.9	45.1	0.39
8	13	345.8	24.0	201.0	41.1	55.5	44.5	0.29
g	12	349.2	25.6	205.9	40.8	54.6	45.4	0.30
10	10	344.6	17.9	197.1	36.6	56.3	43.7	0.36
11	10	346.1	22.3	198.0	42.2	56.4	43.6	0.11
12	6	356.9	25.1	206.6	37.5	54.1	45.9	0.29
13	5	350.3	19.6	197.3	41.6	55.2	44.8	0.10
avg^{b}		344.5	24.8	198.1	40.5	57.5	42.3	0.34
STD [€]		5.4	5.4	5.3	2.8	3.0	3.0	0.14
MD^d		337.5	27.4	137.0	32.9	66.7	33.3	0.74

^aThirteen different combinations of *J*-couplings used to model ring conformation; the *J*-values used in each fit are given in Table S4 in the Supporting Information. ^bAveraged values obtained from the 13 *MA'AT* fits. ^cSTD = standard deviation. ^dObtained from a 1 μ s aqueous molecular dynamics simulation of 4 (see text for details). ^eMean 1 and CSD 1 were calculated from peak 1; mean 2 and CSD 2 were calculated from peak 2. ^fObtained from integration of peaks 1 and 2 obtained from *MA'AT* modeling or MD simulation. ^gRMSD = root-mean-square deviation.

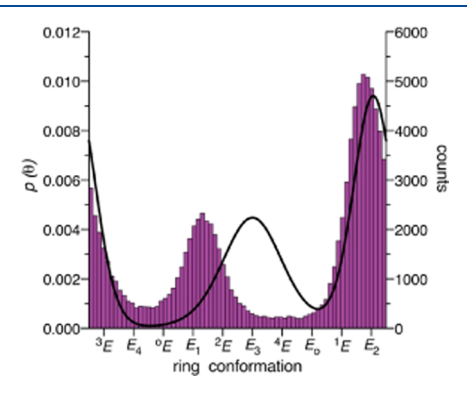


Figure 4. Overlay of the MA'AT model of furanose conformation in 4 with that derived from aqueous molecular dynamics simulation (1 μ s; GLYCAM06). The black curve represents an averaged MA'AT model calculated by combining 13 models obtained from the fits of different ensembles of J-couplings (see Figure 2 and Table 5). The hatched area in purple denotes the MD model.

corresponding J-couplings were compared (Table 6). The results showed that many of the J-couplings in 3 and 4 differ in the two models, although the differences were modest in some cases. For example, 9 vicinal spin couplings in 3 and 11 in 4 show differences ranging from 0.8 to 2.4 Hz. The ensembles of backcalculated *I*-couplings in Table 6 were then used as input in MA'AT analyses to determine whether the analyses would return the same models from which the J-couplings were backcalculated. Both single-state models for 3 and 4 were reproduced almost exactly by MA'AT, while statistical parameters determined for the two-state MA'AT models of 3 and 4 were virtually identical to those expected (see Table S5 in the Supporting Information). For both 3 and 4, MA'AT fits of the back-calculated J-couplings gave the lowest RMSDs for the model from which the back-calculated J-couplings were originally obtained, demonstrating that MA'AT can distinguish between the one- and two-state models.

Studies were then conducted to determine whether *MA'AT* can distinguish between the one- and two-state conformational

Table 6. Back-Calculated Spin-Coupling Constants for One-(°E) and Two-State (${}^3E \leftrightarrows {}^2E$) Conformational Models of 3 and 4^a

methyl β-1	-ribofurano	side (3)	methyl 2-deoxy- β -D-erythropentofuranoside (4)			
J-coupling	1-state	2-state	J-coupling	1-state	2-state	
$^{3}J_{\rm H1,H2}$	4.10	3.33	$^{2}J_{H2R,H2S}$	-13.97	-13.29	
$^{3}J_{H2,H3}$	8.63	6.23	³ J _{H1,H2R}	6.24	5.45	
³ J _{H3,H4}	6.02	4.70	³J _{н1,н2s}	5.88	4.56	
² J _{C1,H2}	-3.14	-2.15	$^{3}J_{H2R,H3}$	3.64	4.95	
$^{2}J_{C2,H1}$	-0.17	-0.35	³ J _{н2S,Н3}	9.76	7.08	
$^{2}J_{C2,H3}$	1.61	1.52	³ J _{H3,H4}	5.66	4.46	
$^{2}J_{C3,H2}$	1.31	1.74	$^{1}J_{C1,H1}$	169.24	172.78	
$^{2}J_{C4,H3}$	0.27	1.29	$^{2}J_{C1,H2R}$	-0.07	0.30	
$^{3}J_{C5,H4}$	0.37	0.71	$^{2}J_{C1,H2S}$	-5.82	-4.85	
$^{3}J_{C1,H3}$	3.30	3.33	$^{2}J_{C2,H3}$	0.23	0.44	
$^{3}J_{C1,H4}$	-0.19	1.85	$^{2}J_{C3,H2R}$	-4.84	-4.96	
$^{3}J_{C2,H4}$	1.03	1.51	$^{2}J_{C3,H2S}$	-1.66	-1.17	
$^{3}J_{C3,H1}$	0.41	1.11	$^{2}J_{C4,H3}$	0.08	1.39	
$^{3}J_{\text{C4,H1}}$	0.03	2.44	$^{3}J_{C1,H3}$	2.96	3.50	
$^3J_{C4,H2}$	3.40	2.97	$^{3}J_{C1,H4}$	-0.16	2.23	
$^{3}J_{C5,H3}$	4.55	3.86	$^{3}J_{C2,H4}$	1.27	1.22	
$^{2}J_{C3,C5}$	1.06	1.80	$^{3}J_{C3,H1}$	0.49	1.60	
$^{3}J_{C1,C5}$	3.62	1.52	$^{3}J_{C4,H1}$	0.03	2.47	
$^{3}J_{C2,C5}$	2.21	1.40	$^{3}J_{C4,H2R}$	1.35	2.60	
$^{2+3}J_{C1,C3}$	4.69	4.41	$^{3}J_{C4,H2S}$	3.87	3.88	
$^{2+3}J_{C1,C4}$	2.72	1.17	$^{3}J_{C5,H3}$	4.62	3.94	
²⁺³ J _{C2,C4}	1.75	2.38	$^{2}J_{C3,C5}$	1.42	2.16	
			³ J _{C1,C5}	3.99	1.70	
			$^{3}J_{C2,C5}$	2.30	1.54	
			$^{2+3}J_{C1,C3}$	2.51	2.16	
			2+3J _{C1.C4}	3.08	1.58	
			$^{2+3}J_{C2,C4}$	1.41	2.02	
an .1 .		1.1	1 1	c 3m	1 2 17	

"For the two-state model, equal populations of ³E and ²E were assumed. CSDs for all peaks were set at 30°. See text for details.

models of 3 and 4 described above and a more complex threestate model in which ${}^{3}E$ ($P = 18^{\circ}$), ${}^{\circ}E$ ($P = 90^{\circ}$), and ${}^{2}E$ ($P = 90^{\circ}$) 162°) are equally populated. CSDs of each population were assumed to be either 10 or 30°. Back-calculated J-couplings for the three-state model were first obtained and then used as input in MA'AT analysis. MA'AT recapitulated the three-state model accurately when the fit was constrained to three states. However, if the fit of the three-state back-calculated J-couplings was constrained to two states, a two-state N/S model was returned that had a lower RMSD than the three-state fit. Thus, MA'AT was not able to identify the three-state model unambiguously. Further studies showed that this behavior may be due (a) to the particular three-state model chosen for the calculations where equal populations of each state were assumed and (b) to the fact that ${}^{\circ}E$ is located exactly between the assumed ${}^{3}E$ and ${}^{2}E$ forms. Results not shown here suggest that some three-state models in which one state is °E may be unambiguously determined by MA'AT, especially when the three states are not equally populated and/or when the north and south states are not equally displaced from °E along the pseudorotational itinerary (e.g., an $E_2 \leq {}^{\circ}E \leq {}^{2}E$ equilibrium).

These studies, although limited in scope, suggest that while any given J-coupling may exhibit small or modest changes in different conformational models, the collective changes that occur in multiple J-couplings between different models appear to be the key factor in enabling MA'AT analysis to discriminate between different models. In the present case, the degree to which MA'AT analysis is able to discriminate between one- and two-state models of 3 and 4 depends on the accuracy of the measured J-values used in the analyses, with J-couplings having errors of ± 0.1 Hz or smaller desirable. In relatively small molecules, this level of accuracy is achievable if high-quality NMR data are available and second-order effects are taken into account, but accuracy is likely to suffer as the molecular weight of the molecule increases due to complications arising from increasing correlation times and resonance line-widths.

CONCLUSIONS

Conformational analysis of oligoribonucleotides and oligodeoxyribonucleotides requires treatment of furanose ring conformation. Historically, ${}^3J_{\rm HH}$ values have been used in this treatment, ${}^{4,13,14,16,66-68}$ although efforts have been made to include heteronuclear $J_{\rm CH}$ values, at least qualitatively. Given the limited number of ³J_{HH} values available in ribo (1) and 2deoxyribo rings (2) and the large number of conformational states available to these rings, conformational modeling is not possible without invoking assumptions about the nature of the model (i.e., confine experimental data analysis to two-state N/Smodels). It has not been possible to allow the experimental data to dictate the model without bias or to avoid fitting a modest number of experimental constraints to models determined by MD simulation. The same limitations apply to the conformational analysis of aldofuranosyl rings having other ring configurations, such as α/β -arabino, α/β -lyxo, and α/β -xylo. 66 Do the latter rings adopt two-state N/S models in solution or do other models pertain? Recent MD simulations suggest that N/S models that apply to 3 and 4 are probably not adopted universally by rings having different configurations.

The approach described in this study allows probability distribution modeling of aldofuranosyl ring pseudorotation in solution based solely on experimental inputs. The *MA'AT* method is well suited to furanosyl ring conformational analysis since these rings contain large numbers of redundant spin-

coupling constants that display strong dependencies on ring conformation, which renders multi-state MA'AT modeling feasible.

MA'AT analysis of the β -ribo (3) and 2-deoxy- β -ribo (4) rings provides new experimental validation of the two-state N/S models commonly invoked for these rings, at least for those free in solution. The MA'AT results show that the mean values of the pseudorotation phase angles P for 3 are in good agreement with those obtained by MD simulation, and that relative populations of the N and S forms determined by MA'AT are very similar to those predicted by MD. MA'AT analysis of 3 indicates that averaging about the two mean P values is more restricted than that predicted by MD. In multi-state modeling with MA'AT described herein and in unpublished work, mean values of molecular torsion angles (in the present case embodied in *P*) have been found to be very reliable, whereas CSDs are less so. Thus, while the MA'AT analysis suggests more restricted conformational averaging for 3 than found by MD, this finding would benefit from additional experimental validation.

Westhof and Sundaralingam⁷⁴ have shown that hydroxylation of furanose and pyrrolidine (proline) rings results in decreased flexibility. This assertion refers to the activation barrier to N/S exchange, with that associated with β -ribo or hydroxyproline rings higher than those associated with 2-deoxy-β-ribo and proline rings. The present work does not speak to differences in activation barriers for N/S exchange but does provide new experimental evidence that less librational averaging around the preferred values of P is observed for an unsubstituted β -Dribofuranoside than for an unsubstituted 2-deoxy-β-D-erythropentofuranoside in the aqueous (${}^{2}H_{2}O$) solution. Apparently, the loss of the 2-hydroxyl group renders the furanose ring more flexible. While multiple factors may be responsible for this behavior, the presence of vicinal hydroxyl groups in 3 may potentially constrain motion through intramolecular or intermolecular (with solvent water) hydrogen bonding. Recent conformational studies of 3 using rotational spectra in a supersonic jet expansion show that its furanosyl ring adopts a N conformation (near 3T_2) in the gas phase almost exclusively. ⁷⁵ Thus, in the absence of the solvent, north geometries of 3 are intrinsically favored. MA'AT modeling shows that, while N forms of 3 dominate (77%), a substantial population of the S form (23%) exists in the aqueous (${}^{2}H_{2}O$) solution. These results suggest that solvation may preferentially stabilize S forms of the ring, possibly through more potent intermolecular hydrogen bonding in the latter and/or to altered strengths of competing stereoelectronic effects (anomeric and gauche) within the ring.

MA'AT models of 3 and 4 show that both rings adopt twostate models, but the two dominant ring conformers in each model differ, especially for the S forms. Conventional PSEUROT analyses of ${}^3J_{\rm HH}$ values in 3 yielded a two-state N/S model in $^{2}\text{H}_{2}\text{O}$ with $P(N) = 344^{\circ}$ (E_{2}), $P(S) = 158^{\circ}$ (^{2}E), and 94% N forms, ⁶⁸ compared to values of 355°, 179°, and 77%, respectively (Table 4) determined by MA'AT analysis. Like PSEUROT, MA'AT analysis indicates that the N form is preferred in solution, although it is less abundant than indicated by PSEUROT. X-ray crystal structures of 3 contain two ring conformations, one with $P = 349^{\circ}$ and the other with $P = 336^{\circ}$, consistent with E_2 ring conformations.^{71,76} The dominant conformer observed in the solution is the same form as that observed in the crystal. Conventional PSEUROT analyses of $^{3}J_{\rm HH}$ values in 4 support a two-state N/S model in $^{2}H_{2}O$, with $P(N) = 335^{\circ} (E_2), P(S) = 211/234^{\circ} ({}^{4}T_3/{}^{4}E), \text{ and } 52-60\% N$ forms, ^{68,77} compared to values of 345°, 198°, and 58%,

respectively (Table 5) determined by MA'AT analysis. Given the uncertainties in both the PSEUROT and MA'AT treatments, the agreement between the two methods is very good for 4, supporting the contention that a more equal distribution of N and S conformers exists in aqueous solutions of 4 compared to solutions of 3 where the N form is the more favored.

MA'AT and MD models of the 2-deoxy- β -ribo ring 4 were found to differ with regard to the mean values of P and N/S equilibria. The discrepancy is particularly significant for the mean P-value of the S form. These results suggest that the GLYCAM06 force field may not be parameterized to accurately predict the solution behavior of this ring. With regard to CSDs, however, the MA'AT and MD data for 4 are in good agreement, unlike what was observed for 3.

The probability distribution models obtained from MA'AT analyses of 3 and 4 show north and south conformer populations that range from 20 to 80%. However, two-state furanose ring conformational equilibria may occur wherein one of the states is minimally populated. Based on general tests of the MA'AT method using contrived two-state equilibria, the lower limit of detection of a conformer population is likely to be $\sim 10\%$. This limit is partly determined by the number of J-couplings used in the analysis and the degree to which they depend on a given torsion angle. J-Couplings with large dynamic ranges and minimal secondary dependencies on structure lead to more accurate fits of the data, which in turn may lower the detection limit of minor populations.

The studies described herein focused on simple furanose rings to test the multi-state modeling capabilities of MA'AT analysis. Prior work using the MA'AT method treated systems in which single-state conformational models gave best fits of the spincoupling data.²⁶⁻³⁰ Application of the MA'AT method to the furanosyl rings of oligonucleotides may provide greater clarity on the conformational behaviors of these rings in both singlestranded and duplex structures. The ability of the method to distinguish between single-state east models and typical N/S two-state models may be particularly useful in studies of RNA-DNA duplexes, where aberrant furanose ring conformations may exist. 65 Future applications of MA'AT analysis to furanose rings in oligonucleotides will require determinations of the effects of phosphate ester functionality on *J*-coupling behavior in β -ribo (1) and 2-deoxy- β -ribo (2) rings. The equations reported herein for 3 and 4 may not be applicable to these phosphorylated systems. Furthermore, measurements of large ensembles of ring *I*-couplings may be challenging in oligonucleotides. Preliminary studies of an ensemble of nine *J*-couplings in 3 and 4 that were chosen because of their expected relative ease of measurement in these systems showed that, for 3, the resulting model was very similar to that shown in Figure 2, giving comparable mean P values for the N and S conformers and similar relative populations, although the CSDs were smaller (Figure S6A, Supporting Information). Similar results were obtained for 4, and in this case, the CSDs for both models were similar (Figure S6B, Supporting Information). These initial findings suggest that, even when access to redundant *J*-values is limited, reliable MA'AT models of furanose ring conformation in oligonucleotides should be obtainable. In these larger systems, errors in the experimental *I*-couplings will increase. However, even with errors of up to ± 0.5 Hz, preliminary work indicates that reliable MA'AT models can still be obtained, especially when the dynamic ranges of the J-couplings used in the analysis are relatively large. Additional study will be needed to fully define the limits of MA'AT analysis as applied to oligonucleotides.

Likewise, characterizing the pseudorotational properties of sixmembered pyranosyl rings remains an experimental problem that *MA'AT* analysis may be able to address, especially in cases where conformational heterogeneity is expected.⁷⁸

ASSOCIATED CONTENT

Supporting Information

The Supporting Information is available free of charge at https://pubs.acs.org/doi/10.1021/acs.biochem.1c00630.

Summary of torsion angle constraints used in DFT calculations of 3° (Scheme S1); summary of torsion angle constraints used in DFT calculations of 4^c (Scheme S2); initial and optimized puckering parameters in 3° and 4° (Table S1); mean exocyclic torsion angles in 3° and 4° (Table S2); DFT-parameterized spin-coupling equations (eqs S1–S26): methyl β -D-ribofuranoside (3°); DFTparameterized spin-coupling equations (eqs S27–S58): methyl 2-deoxy- β -D-erythro-pentofuranoside (4°); plots of calculated vicinal ¹H-¹H spin couplings in 3^c and 4^c as a function of P (Figure S1); plots of calculated geminal $^{13}\text{C}-^{1}\text{H}$ spin couplings in 3° and 4° as a function of P (Figure S2); plots of calculated vicinal ¹³C-¹H spin couplings in 3^{c} and 4^{c} as a function of P (Figure S3); plots of calculated geminal, vicinal and dual-pathway ¹³C-¹³C spin couplings in 3^{c} and 4^{c} as a function of P (Figure S4); plot of calculated ${}^{2}J_{C4,H3}$ in 4 as a function of endocyclic torsion angle C2-C3-C4-O4 (Figure S5); ensembles of redundant spin couplings used in MA'AT modeling of methyl β -D-ribofuranoside (3) (Table S3); ensembles of redundant spin couplings used in MA'AT modeling of methyl 2-deoxy- β -D-erythro-pentofuranoside (4) (Table S4); statistics for MA'AT models of 3 and 4 using backcalculated *J*-couplings in two-state (${}^{3}E \iff {}^{2}E$) models (Table S5); MA'AT analysis of 3 and 4 using nine spin couplings relevant to oligonucleotides (Figure S6); brief description of the MA'AT algorithm; and representative Cartesian coordinates for 3° and 4° (PDF)

AUTHOR INFORMATION

Corresponding Author

Anthony S. Serianni — Department of Chemistry and Biochemistry, University of Notre Dame, Notre Dame, Indiana 46556-5670, United States; o orcid.org/0000-0001-6114-1446; Email: aseriann@nd.edu

Authors

Reagan J. Meredith — Department of Chemistry and Biochemistry, University of Notre Dame, Notre Dame, Indiana 46556-5670, United States

Margaret McGurn – Department of Chemistry and Biochemistry, University of Notre Dame, Notre Dame, Indiana 46556-5670, United States

Christopher Euell – Department of Chemistry and Biochemistry, University of Notre Dame, Notre Dame, Indiana 46556-5670, United States

Peter Rutkowski — Department of Chemistry and Biochemistry, University of Notre Dame, Notre Dame, Indiana 46556-5670, United States

Evan Cook – Department of Chemistry and Biochemistry, University of Notre Dame, Notre Dame, Indiana 46556-5670, United States Ian Carmichael – Radiation Laboratory, University of Notre Dame, Notre Dame, Indiana 46556-5670, United States

Complete contact information is available at: https://pubs.acs.org/10.1021/acs.biochem.1c00630

Notes

The authors declare no competing financial interest.

ACKNOWLEDGMENTS

This work was supported by the National Science Foundation (CHE 1707660 and CHE 2002625 to A. Serianni) and by Omicron Biochemicals, Inc., South Bend, IN. The Notre Dame Radiation Laboratory is supported by the Department of Energy Office of Science, Office of Basic Energy Sciences, under Award Number DE-FC02-04ER15533. This is document number NDRL 5328.

REFERENCES

- (1) Nussinov, R.; Udgaonkar, J.; Lilley, D.; Pyle, A. M., Eds. Folding and Binding—Nucleic Acids—Protein Complexes. *Current Opinion in Structural Biology*; Elsevier, 2016; Vol. 36, pp 1–148.
- (2) Fry, C. J.; Farnham, P. J. Context-dependent Transcriptional Regulation. J. Biol. Chem. 1999, 274, 29583–29586.
- (3) Hwang, S.; Kim, S.; Shin, H.; Lee, D. Context-dependent Transcriptional Regulations Between Signal Transduction Pathways. *BMC Bioinf.* **2011**, *12*, No. 19.
- (4) Saenger, W.Principles of Nucleic Acid Structure; Springer-Verlag: New York, 1984.
- (5) Sokoloski, J. E.; Godfrey, S. A.; Dombrowski, S. E.; Bevilacqua, P. C. Prevalance of *syn* Nucleobases in the Active Sites of Functional RNAs. *RNA* **2011**, *17*, 1775–1787.
- (6) Olson, W. K. How Flexible is the Furanose Ring? 2. An Updated Potential Energy Estimate. *J. Am. Chem. Soc.* **1982**, *104*, 278–286.
- (7) Harvey, S. C.; Prabhakaran, M. Ribose Puckering: Structure, Dynamics, Energetics and the Pseudorotation Cycle. *J. Am. Chem. Soc.* **1986**, *108*, 6128–6136.
- (8) Cloran, F.; Carmichael, I.; Serianni, A. S. ¹³C-¹H and ¹³C-¹³C Spin-Coupling Behavior in Aldofuranosyl Rings from Density Functional Theory. *J. Phys. Chem. A* **1999**, *103*, 3783–3795.
- (9) Tolstorukov, M. Y.; Jernigan, R. L.; Zhurkin, V. B. Protein-DNA Hydrophobic Recognition in the Minor Groove Is Facilitated By Sugar Switching. *J. Mol. Biol.* **2004**, *337*, 65–76.
- (10) Mei, H.-Y.; Kaaret, T. W.; Bruice, T. C. A Computational Approach to the Mechanism of Self-cleavage of Hammerhead RNA. *Proc. Natl. Acad. Sci. U.S.A.* **1989**, *86*, 9727–9731.
- (11) White, N. A.; Sumita, M.; Marquez, V. E.; Hoogstraten, C. G. Coupling Between Conformational Dynamics and Catalytic Function at the Active Site of the Lead-dependent Ribozyme. *RNA* **2018**, *24*, 1542–1554.
- (12) Podlasek, C. A.; Stripe, W. A.; Carmichael, I.; Shang, M.; Basu, B.; Serianni, A. S. 13 C- 1 H Spin-Coupling Constants in the β -D-Ribofuranosyl Ring: Effect of Ring Conformation on Coupling Magnitudes. *J. Am. Chem. Soc.* **1996**, *118*, 1413–1425.
- (13) Haasnoot, C. A. G.; De Leeuw, F. A. A. M.; De Leeuw, H. P. M.; Altona, C. The Relationship Between Proton-Proton NMR Coupling Constants and Substituent Electronegativities. II. Conformational Analysis of the Sugar Ring in Nucleosides and Nucleotides in Solution Using a Generalized Karplus Equation. *Org. Magn. Reson.* 1981, 15, 43—52.
- (14) Wüthrich, K.NMR of Proteins and Nucleic Acids; Wiley, 1991.
- (15) Hendrickx, P. M. S.; Martins, J. C. A User-friendly *Matlab* Program and GUI for the Pseudorotation Analysis of Saturated Five-membered Ring Systems Based on Scalar Coupling Constants. *Chem. Cent. J.* 2008, 2, No. 20.
- (16) Boisbouvier, J.; Brutscher, B.; Pardi, A.; Marion, D.; Simorre, J.-P. NMR Determination of Sugar Puckers in Nucleic Acids from CSA-

- Dipolar Cross-Correlated Relaxation. J. Am. Chem. Soc. 2000, 122, 6779-6780.
- (17) Felli, I. C.; Richter, C.; Griesinger, C.; Schwalbe, H. Determination of RNA Sugar Pucker Mode from Cross-Correlated Relaxation in Solution NMR Spectroscopy. *J. Am. Chem. Soc.* **1999**, *121*, 1956–1957.
- (18) De Leeuw, F. A. A. M.; Altona, C. Computer-assisted Pseudorotation Analysis of Five-membered Rings by Means of Proton Spin—Spin Coupling Constants: Program *PSEUROT. J. Comput. Chem.* **1983**, *4*, 428–437.
- (19) De Leeuw, F. A. A. M.; van Beuzekom, A. A.; Altona, C. Throughspace Effects on Vicinal Proton Spin-spin Coupling Constants Mediated via Hetero Atoms: Nonequivalence of *cis* Couplings in Five-membered Rings. *J. Comput. Chem.* **1983**, *4*, 438–448.
- (20) Barfield, M. Nuclear Spin-spin Coupling via Nonbonded Interactions. 1. Conformational and Substituent Effects on Vicinal Carbon-13-Proton and Carbon-13-Carbon-13 Coupling Constants. *J. Am. Chem. Soc.* **1980**, *102*, 1–7.
- (21) Olson, W. K. Three-state Models of Furanose Pseudorotation. *Nucleic Acids Res.* **1981**, *9*, 1251–1262.
- (22) Zhu, G.; Live, D.; Bax, A. Analysis of Sugar Puckers and Glycosidic Torsion Angles in a DNA G-tetrad Structure by Heteronuclear Three-Bond J Couplings. J. Am. Chem. Soc. 1994, 116, 8370–8371.
- (23) Hines, J. V.; Landry, S. M.; Varani, G.; Tinoco, I., Jr. Carbon-Proton Scalar Couplings in RNA: 3D Heteronuclear and 2D Isotope-Edited NMR of a ¹³C-Labeled Extra-stable Hairpin. *J. Am. Chem. Soc.* **1994**, *116*, 5823–5831.
- (24) Marino, J. P.; Schwalbe, H.; Glaser, S. J.; Griesinger, C. Determination of γ and Stereospecific Assignment of H5' Protons by Measurement of 2J and 3J Coupling Constants in Uniformly 13 C Labeled RNA. *J. Am. Chem. Soc.* **1996**, *118*, 4388–4395.
- (25) Church, T. J.; Carmichael, I.; Serianni, A. S. 13 C- 1 H and 13 C- 13 C Spin-Coupling Constants in Methyl β -D-Ribofuranoside and Methyl 2-Deoxy- β -D-erythro-pentofuranoside: Correlations with Molecular Structure and Conformation. *J. Am. Chem. Soc.* **1997**, *119*, 8946–8964.
- (26) Turney, T.; Pan, Q.; Sernau, L.; Carmichael, I.; Zhang, W.; Wang, X.; Woods, R. J.; Serianni, A. S. *O*-Acetyl Side-chains in Monosacccharides: Redundant NMR Spin-Couplings and Statistical Models for Acetate Ester Conformational Analysis. *J. Phys. Chem. B* **2017**, *121*, 66–77.
- (27) Zhang, W.; Turney, T.; Meredith, R.; Pan, Q.; Sernau, L.; Wang, X.; Hu, X.; Woods, R. J.; Carmichael, I.; Serianni, A. S. Conformational Populations of β -(1 \rightarrow 4) *O*-Glycosidic Linkages Using Redundant NMR *J*-Couplings and Circular Statistics. *J. Phys. Chem. B* **2017**, *121*, 3042-3058.
- (28) Zhang, W.; Meredith, R.; Yoon, M.-K.; Wang, X.; Woods, R. J.; Carmichael, I.; Serianni, A. S. Synthesis and O-Glycosidic Linkage Conformational Analysis of ¹³C-Labeled Oligosaccharide Fragments of an Antifreeze Glycolipid. *J. Org. Chem.* **2019**, *84*, 1706–1724.
- (29) Zhang, W.; Meredith, R.; Pan, Q.; Wang, X.; Woods, R. J.; Carmichael, I.; Serianni, A. S. Use of Circular Statistics To Model α Man- $(1\rightarrow 2)$ - α Man and α Man- $(1\rightarrow 3)\alpha/\beta$ Man O-Glycosidic Linkage Conformation in 13 C-Labeled Disaccharides and High-Mannose Oligosaccharides. *Biochemistry* **2019**, *58*, 546–560.
- (30) Meredith, R. J.; Woods, R. J.; Carmichael, I.; Serianni, A. S. Reconciling *MA'AT* and Molecular Dynamics Models of Linkage Conformation in Oligosaccharides. *Phys. Chem. Chem. Phys.* **2020**, 22, 14454–14457.
- (31) Frisch, M. J.; Trucks, G. W.; Schlegel, H. B.; Scuseria, G. E.; Robb, M. A.; Cheeseman, J. R.; Scalmani, G.; Barone, V.; Petersson, G. A.; Nakatsuji, H.; Li, X.; Caricato, M.; Marenich, A. V.; Bloino, J.; Janesko, B. G.; Gomperts, R.; Mennucci, B.; Hratchian, H. P.; Ortiz, J. V.; Izmaylov, A. F.; Sonnenberg, J. L.; Williams-Young, D.; Ding, F.; Lipparini, F.; Egidi, F.; Goings, J.; Peng, B.; Petrone, A.; Henderson, T.; Ranasinghe, D.; Zakrzewski, V. G.; Gao, J.; Rega, N.; Zheng, G.; Liang, W.; Hada, M.; Ehara, M.; Toyota, K.; Fukuda, R.; Hasegawa, J.; Ishida, M.; Nakajima, T.; Honda, Y.; Kitao, O.; Nakai, H.; Vreven, T.; Throssell, K.; Montgomery, J. A., Jr.; Peralta, J. E.; Ogliaro, F.; Bearpark,

- M. J.; Heyd, J. J.; Brothers, E. N.; Kudin, K. N.; Staroverov, V. N.; Keith, T. A.; Kobayashi, R.; Normand, J.; Raghavachari, K.; Rendell, A. P.; Burant, J. C.; Iyengar, S. S.; Tomasi, J.; Cossi, M.; Millam, J. M.; Klene, M.; Adamo, C.; Cammi, R.; Ochterski, J. W.; Martin, R. L.; Morokuma, K.; Farkas, O.; Foresman, J. B.; Fox, D. J. Gaussian 16, revision B.01; Gaussian, Inc.: Wallingford, CT, 2016.
- (32) Becke, A. D. Density-Functional Thermochemistry. III. The Role of Exact Exchange. *J. Chem. Phys.* **1993**, *98*, 5648–5652.
- (33) Becke, A. D. New Mixing of Hartree-Fock and Local Density-Functional Theories. *J. Chem. Phys.* **1993**, 98, 1372–1377.
- (34) Hehre, W. J.; Ditchfield, R.; Pople, J. A. Self-Consistent Molecular Orbital Methods. XII. Further Extensions of Gaussian-Type Basis Sets for Use in Molecular Orbital Studies of Organic Molecules. *J. Chem. Phys.* **1972**, *56*, 2257–2261.
- (35) Altona, C.; Sundaralingam, M. Conformational Analysis of the Sugar Ring in Nucleosides and Nucleotides. New Description Using the Concept of Pseudorotation. *J. Am. Chem. Soc.* **1972**, *94*, 8205–8212.
- (36) Westhof, E.; Sundaralingam, M. A Method for the Analysis of Puckering Disorder in Five-Membered Rings: The Relative Mobilities of Furanose and Proline Rings and Their Effects on Polynucleotide and Polypeptide Backbone Flexibility. *J. Am. Chem. Soc.* **1983**, *105*, 970–976.
- (37) Cancès, E.; Mennucci, B.; Tomasi, J. A New Integral Equation Formalism for the Polarizable Continuum Model: Theoretical Background and Applications To Isotropic and Anisotropic Dielectrics. *J. Chem. Phys.* **1997**, *107*, 3032–3041.
- (38) Cammi, R.; Mennucci, B.; Tomasi, J. Fast Evaluation of Geometries and Properties of Excited Molecules in Solution: A Tamm-Dancoff Model with Application to 4-Dimethyl- aminobenzonitrile. *J. Phys. Chem. A* **2000**, *104*, 5631–5637.
- (39) Sychrovský, V.; Grafenstein, J.; Cremer, D. Nuclear Magnetic Resonance Spin—Spin Coupling Constants from Coupled Perturbed Density Functional Theory. *J. Phys. Chem. A* **2000**, *113*, 3530—3547.
- (40) Helgaker, T.; Watson, M.; Handy, N. C. Analytical Calculation of Nuclear Magnetic Resonance Indirect Spin—Spin Coupling Constants at the Generalized Gradient Approximation and Hybrid Levels of Density-Functional Theory. *J. Chem. Phys.* **2000**, *113*, 9402—9409.
- (41) Barone, V.; Peralta, J. E.; Contreras, R. H.; Snyder, J. P. DFT Calculation of NMR $J_{\rm FF}$ Spin Spin Coupling Constants in Fluorinated Pyridines. *J. Phys. Chem. A* **2002**, *106*, 5607–5612.
- (42) Klepach, T.; Zhao, H.; Hu, X.; Zhang, W.; Stenutz, R.; Hadad, M. J.; Carmichael, I.; Serianni, A. S.Informing Saccharide Structural NMR Studies with Density Functional Theory Calculations. In *Glycoinformatics: Methods in Molecular Biology*; Lütteke, T.; Frank, M., Eds.; Springer: New York, 2015; pp 289–331.
- (43) Stenutz, R.; Carmichael, I.; Widmalm, G.; Serianni, A. S. Hydroxymethyl Group Conformation in Saccharides: Structural Dependencies of ${}^2J_{\rm HH}$, ${}^3J_{\rm HH}$ and ${}^1J_{\rm CH}$ Spin-Spin Coupling Constants. *J. Org. Chem.* **2002**, *67*, 949–958.
- (44) Pachler, K. G. R. Extended Hückel Theory MO Calculations of Proton-Proton Coupling Constants—II: The Effect of Substituents on Vicinal Couplings in Monosubstituted Ethanes. *Tetrahedron* 1971, 27, 187–199.
- (45) Complex Carbohydrate Research Center (CRCC), University of Georgia. http://www.glycam.org
- (46) Kirschner, K. N.; Yongye, A. B.; Tschampel, S. M.; González-Outeiriño, J.; Daniels, C. R.; Foley, B. L.; Woods, R. J. GLYCAM06: A Generalizable Biomolecular Force Field. Carbohydrates. *J. Comput. Chem.* **2008**, *29*, 622–655.
- (47) Jorgensen, W. L.; Chandrasekhar, J.; Madura, J. D.; Impey, R. W.; Klein, M. L. Comparison of Simple Potential Functions for Simulating Liquid Water. *J. Chem. Phys.* **1983**, *79*, 926–935.
- (48) Case, D. A.; Babin, V.; Berryman, J. T.; Betz, R. M.; Cai, Q.; Cerutti, D. S.; Cheatham, T. E. I.; Darden, T. A.; Duke, R. E.; Gohlke, H.; Goetz, A. W.; Gusarov, S.; Homeyer, N.; Janowski, P.; Kaus, J.; Kolossváry, I.; Kovalenko, A.; Lee, T. S.; LeGrand, S.; Luchko, T.; Luo, R.; Madej, B.; Merz, K. M.; Paesani, F.; Roe, D. R.; Roitberg, A.; Sagui, C.; Salomon-Ferrer, R.; Seabra, G.; Simmerling, C. L.; Smith, W.;

- Swails, J.; Walker, R. C.; Wang, J.; Wolf, R. M.; Wu, X.; Kollman, P. A. AMBER 14; University of California: San Francisco, 2014.
- (49) Berendsen, H. J. C.; Postma, J. P. M.; van Gunsteren, W. F.; DiNola, A.; Haak, J. R. Molecular Dynamics With Coupling to an External Bath. *J. Chem. Phys.* **1984**, *81*, 3684–3690.
- (50) van Gunsteren, W. F.; Berendsen, H. J. C. Algorithms for Macromolecular Dynamics and Constraint Dynamics. *Mol. Phys.* **1977**, 34, 1311–1327.
- (51) Götz, A. W.; Williamson, M. J.; Xu, D.; Poole, D.; Le Grand, S.; Walker, R. C. Routine Microsecond Molecular Dynamics Simulations with AMBER on GPUs. 1. Generalized Born. *J. Chem. Theory Comput.* **2012**, *8*, 1542–1555.
- (52) Kirschner, K. N.; Woods, R. J. Solvent Interactions Determine Carbohydrate Conformation. *Proc. Natl. Acad. Sci. U.S.A.* **2001**, 98, 10541–10545.
- (53) Prism 8 for Mac OS X, version 8.4.2 (464); GraphPad Software, April 18, 2020.
- (54) Karplus, M. Contact Electron-Spin Coupling of Nuclear Magnetic Moments. J. Chem. Phys. 1959, 30, 11–15.
- (55) Mulloy, B.; Frenkiel, T.; Davies, D. B. Long-range Carbon-Proton Coupling Constants: Application To Conformational Studies of Oligosaccharides. *Carbohydr. Res.* 1988, 184, 39–46.
- (56) Tvaroska, I.; Taravel, F. R.Carbon-Proton Coupling Constants in the Conformational Analysis of Sugar Molecules. *Advances in Carbohydrate Chemistry and Biochemistry*; Academic Press, Inc., 1995; Vol. 51, pp 15–61.
- (57) Bose, B.; Zhao, S.; Bondo, P.; Bondo, G.; Cloran, F.; Carmichael, I.; Stenutz, R.; Hertz, B.; Serianni, A. S. Three-Bond C-O-C-C Spin-Coupling Constants in Carbohydrates: Development of a Karplus Relationship. *J. Am. Chem. Soc.* **1998**, *120*, 11158–11173.
- (58) Serianni, A. S.; Wu, J.; Carmichael, I. One-Bond ¹³C-¹H Spin-Coupling Constants in Aldofuranosyl Rings: Effect of Conformation on Coupling Magnitude. *J. Am. Chem. Soc.* **1995**, *117*, 8645–8650.
- (59) Müller, N.; Prtichard, D. E. C13 Splittings in Proton Magnetic Resonance Spectra. I. Hydrocarbons. *J. Chem. Phys.* **1959**, 31, 768–771.
- (60) Cloran, F.; Zhu, Y.; Osborn, J.; Carmichael, I.; Serianni, A. S. 2-Deoxy-β-D-ribofuranosylamine: Quantum Mechanical Calculations of Molecular Structure and NMR Spin-Spin Coupling Constants in Nitrogen-Containing Saccharides. *J. Am. Chem. Soc.* **2000**, *122*, 6435–6448
- (61) Carmichael, I.; Chipman, D. M.; Podlasek, C. A.; Serianni, A. S. Torsional Effects on the One-Bond ^{13}C - ^{13}C Spin Coupling Constant in Ethylene Glycol: Insights Into the Behavior of $^{1}J_{\text{CC}}$ in Carbohydrates. *J. Am. Chem. Soc.* **1993**, *115*, 10863–10870.
- (62) Klepach, T. E.; Carmichael, I.; Serianni, A. S. Geminal ${}^2J_{\text{CCH}}$ Spin-Spin Coupling Constants as Probes of the ϕ Glycosidic Torsion Angle in Oligosaccharides. *J. Am. Chem. Soc.* **2005**, *127*, 9781–9793.
- (63) Bose-Basu, B.; Klepach, T.; Bondo, G.; Bondo, P. B.; Zhang, W.; Carmichael, I.; Serianni, A. S. ¹³C-¹³C NMR Spin-Spin Coupling Constants in Saccharides: Structural Correlations Involving All Carbons In Aldopyranosyl Rings. *J. Org. Chem.* **2007**, *72*, 7511–7522.
- (64) Foloppe, N.; MacKerell, A. D., Jr. Conformational Properties of the Deoxyribose and Ribose Moieties of Nucleic Acids: A Quantum Mechanical Study. *J. Phys. Chem. B* **1998**, *102*, 6669–6678.
- (65) Salazar, M.; Fedoroff, O. Y.; Miller, J. M.; Ribeiro, S.; Reid, B. R. The DNA Strand in DNA.RNA Hybrid Duplexes is Neither B-form nor A-form in Solution. *Biochemistry* **1993**, *32*, 4207–4215.
- (66) Houseknecht, J. B.; Altona, C.; Hadad, C. M.; Lowary, T. L. Conformational Analysis of Furanose Rings with *PSEUROT*: Parameterization for Rings Possessing the *Arabino, Lyxo, Ribo* and *Xylo* Stereochemistry and Application to Arabinofuranosides. *J. Org. Chem.* **2002**, *67*, 4647–4651.
- (67) Szyperski, T.; Fernandez, C.; Ono, A.; Kainosho, M.; Wüthrich, K. Measurement of Deoxyribose ³J_{HH} Scalar Couplings Reveals Protein Binding-Induced Changes in the Sugar Puckers of the DNA. *J. Am. Chem. Soc.* **1998**, *120*, 821–822.
- (68) Raap, J.; van Boom, J. H.; van Lieshout, H. C.; Haasnoot, C. A. G. Conformations of Methyl 2'-Deoxy- α -D-ribofuranoside and Methyl β -

- D-ribofuranoside: A Proton Magnetic Resonance Spectroscopy and Molecular Mechanics Study. J. Am. Chem. Soc. 1988, 110, 2736–2743.
- (69) Hines, J. V.; Landry, S. M.; Varani, G.; Tinoco, I., Jr. Carbon-Proton Scalar Couplings in RNA: 3D Heteronuclear and 2D Isotope-Edited NMR of a ¹³C-Labeled Extra-stable Hairpin. *J. Am. Chem. Soc.* **1994**, *116*, 5823–5831.
- (70) Zhu, G.; Live, D.; Bax, A. Analysis of Sugar Puckers and Glycosidic Torsion Angles in a DNA G-Tetrad Structure by Heteronuclear Three-Bond J Couplings. J. Am. Chem. Soc. 1994, 116, 8370–8371.
- (71) Kline, P. C.; Serianni, A. S. ¹³C-Enriched Ribonucleosides: Synthesis and Application of ¹³C-¹H and ¹³C-¹³C Spin-Coupling Constants To Assess Furanose and N-Glycoside Bond Conformation. J. Am. Chem. Soc. **1990**, 112, 7373–7381.
- (72) Wu, J.; Serianni, A. S. ¹³C-Labeled Oligodeoxyribonucleotides: A Solution Study of a CCAAT-Containing Sequence at the Nuclear Factor I Recognition Site of Human Adenovirus. *Biopolymers* **1994**, *34*, 1175–1186.
- (73) Wang, X.; Woods, R. J. Insights Into Furanose Solution Conformations: Beyond the Two-State Model. *J. Biomol. NMR* **2016**, 64, 291–305.
- (74) Westhof, E.; Sundaralingam, M. A Method For the Analysis of Puckering Disorder in Five-Membered Rings: The Relative Mobilities of Furanose and Proline Rings and Their Effects on Polynucleotide and Polypeptide Backbone Flexibility. *J. Am. Chem. Soc.* **1983**, *105*, 970–976.
- (75) Ecija, P.; Uriarte, I.; Spada, L.; Davis, B. G.; Caminati, W.; Basterretxea, F. J.; Lesarri, A.; Cocinero, E. J. Furanosic Forms of Sugars: Conformational Equilibrium of Methyl β -D-Ribofuranoside. *Chem. Commun.* **2016**, 52, 6241–6244.
- (76) Evdokimov, A.; Gilboa, A. J.; Koetzle, T. F.; Klooster, W. T.; Schultz, A. J.; Mason, S. A.; Albinati, A.; Frolow, F. Structures of Furanosides: Geometrical Analysis of Low-Temperature X-Ray and Neutron Crystal Structures of Five Crystalline Methyl Pentofuranosides. *Acta Crystallogr., Sect. B: Struct. Sci.* **2001**, *57*, 213–220.
- (77) Serianni, A. S.; Kline, P. C.; Snyder, J. R. On the Use of Model Compounds To Assess 2-Deoxy-D-erythro-pentofuranose Conformation at Apyrimidinic Sites in DNA. J. Am. Chem. Soc. 1990, 112, 5886—5887
- (78) Bose-Basu, B.; Zhang, W.; Kennedy, J. L.; Hadad, M. J.; Carmichael, I.; Serianni, A. S. ¹³C-Labeled Idopyranosyl Rings: Effects of Methyl Glycosidation and C6 Oxidation on Ring Conformational Equilibria. *J. Org. Chem.* **2017**, *82*, 1356–1370.

